Planetary and Space Science 240 (2024) 105829

Contents lists available at ScienceDirect

Planetary and Space Science

journal homepage: www.elsevier.com/locate/pss

Asteroid regolith strength: Role of fine-fractions

Christopher Cox *, Julie Brisset, Aracelis Partida, Alexander Madison, Olivia Bitcon

Florida Space Institute, University of Central Florida, 12354 Research Parkway, Orlando FL 32826, USA

ARTICLE INFO

Keywords:
Planetary science
Asteroids
Regolith
Mechanical strength
Small solar system bodies

ABSTRACT

Most smaller asteroids (<1 km diameter) are granular material loosely bound together primarily by self-gravity known as rubble piles. In an effort to better understand the evolution of rubble-pile asteroids, we performed bulk measurements using granular simulant to study the effects of the presence of fine grains on the strength of coarse grains. Our laboratory samples consisted of fine–coarse mixtures of varying percentages of fine grains by volume of the sample. We measured the material's angle of repose, Young's Modulus, angle of internal friction, cohesion, and tensile strength by subjecting the samples to compressive and shear stresses. The coarse grains comprising the fine–coarse mixtures ranged from 1 mm to 20 mm (2 cm) and the fines were sieved to sub-millimeter sizes (<1 mm). The measured angles of repose varied between 32°–45° which increased with increasing fine percentage. In compression, samples generally increased in strength with increasing fine percentage for both confined and unconfined environments. In all cases, the peak strengths were not for purely fine grains but for a mixture of fine and coarse grains. Shear stress measurements yielded angles of internal friction ranging between 25° and 45° with a trend opposite that of the angle of repose, 300–550 Pa for bulk cohesion, and 0.5–1.1 kPa for tensile strength. Using other published works that include data from telescopic and in-situ observations as well as numerical simulations, we discussed the implications of our findings regarding rubble-pile formation, composition, evolution, and disruption. We find that the presence of fine grains in subsurface layers of regolith on an asteroid (confined environment) aids the avoidance of disruption due to impact. However these same fines increase an asteroid's chance to disrupt or deform from high rotation speeds due to reduced grain interlocking. In surface layers (unconfined environments), we find that the presence of fine grains between coarse ones generates stronger cohesion and aids in the prevention of mass loss and surface shedding.

1. Introduction

Ground based (e.g. Busch et al., 2011) and in-situ observations of asteroids (Fujiwara et al., 2006; Lauretta et al., 2019; Watanabe et al., 2019) have shown that some asteroidal bodies are not solid. These asteroids are not observed to be monolithic, but instead loose collections of material (Walsh, 2018). This observation is supported by computer modeling. Current models show that strength limits of these asteroids agree with them being composed of a collection of grains (Sánchez and Scheeres, 2014). Additionally, bulk porosity measurements deduced in these models can only be explained by a collection of grains rather than a solid boulder (Sánchez and Scheeres, 2014). These asteroids are called "rubble-pile asteroids" or "rubble piles" (Walsh, 2018).

Holsapple (2010) describes a spin deformation limit for rubble-pile asteroids. This limit is the rotation speed at which a rubble-pile asteroid will experience deformation and eventually experience structural failure. Scheeres et al. (2010), Sánchez and Scheeres (2014), and Scheeres and Sánchez (2018) (among others) describe forces other than self-gravity that allow some rubble piles to spin above the spin limit without dismantling. For instance, internal friction, the ability of soil to resist shear stress, allows soils to resist deformation and display strength levels higher than liquids.

Sánchez and Scheeres (2014) showed that the presence of fine grain materials in a collection of coarse grains can strengthen a granular body by increasing its bulk cohesion. For this reason, it is plausible that the presence of fine grains within some rubble-pile asteroids is what prevents the rotational breakup. Further, in-situ observations have shown that known rubble piles are composed of grains with a large distribution in sizes from fines to boulders (i.e. Fujiwara et al., 2006; Lauretta et al., 2019). Lauretta et al. (2019) reported that OSIRIS-Rex has confirmed the surface of Bennu contains boulders mixed with fine grains. Lauretta et al. (2022) report data that would indicate sub-millimeter particles on the surface and sub-surface of Bennu. Michikami et al. (2019) reported Hayabusa 2 found that Ryugu also contained

* Corresponding author.
E-mail address: christopher.cox@ucf.edu (C. Cox).

https://doi.org/10.1016/j.pss.2023.105829
Received 30 May 2023; Received in revised form 7 December 2023; Accepted 11 December 2023
Available online 13 December 2023

boulder-fine mixtures with similar particle size distributions on the surface though not necessarily as low as less than 1 mm. Other rubble-pile asteroids, such as Itokawa, were also found to be boulder-fine mixtures though it had a much different particle size distribution and frequency on the surface (Fujiwara et al., 2006).

The mechanical properties of rubble-pile asteroids are not currently well understood. Early modeling of rubble-pile asteroids typically neglected tensile strength or physical bonding between individual components (Walsh, 2018). However, it is now understood that small amounts of cohesion could avoid certain failures of these bodies (Walsh, 2018). Sánchez and Scheeres (2014) report a value of 100 Pa that would allow the at-the-time observed asteroids to avoid rotational breakup. Since then, there have been multiple missions to rubble-pile asteroids (see Fujiwara et al., 2006; Watanabe et al., 2019; Lauretta et al., 2019) which have been better able to directly measure physical and mechanical properties. These missions have produced data that show low values for cohesion in the body and on the surface (i.e. Watanabe et al., 2019; Perry et al., 2022). Though it is understood that tensile strength is nonexistent or negligible in most rubble piles (Walsh, 2018), some asteroids defy the theoretical spin limit of an asteroid with zero tensile strength. These rubble piles are known as fast rotators and require tensile strength and increased cohesion to avoid rotational disruption (Holsapple, 2007). Sánchez and Scheeres (2014) offer estimations for bounds on the tensile strength and angle of internal friction produced through simulations. Brisset et al. (2022) report tensile strength and angle of internal friction values for carbonaceous-type asteroid simulant obtained experimentally.

In an effort to understand how these mixtures behave as bulk material, we performed laboratory measurements using samples of fine–coarse mixtures and quantified the influence of fine grains on the strength of materials simulating rubble-pile asteroids both at the surface (unconfined material) and in sublayers (confined material). Measurements included angle of repose (AOR), Young's Modulus (YM) in compression, and angle of internal friction (AIF) and bulk cohesion in shear. Our laboratory-prepared samples were composed of high-fidelity asteroid regolith simulant (Covey et al., 2016; Metzger et al., 2019). In Section 2, our measurement methods are described and the results gathered from those measurements are presented in Section 3. In Section 4 we discuss the validity and implications of our results, and in Section 5 we conclude our paper while summarizing our findings.

2. Methods

In order to study the influence of fine grains on the mechanical properties of coarse-grained material in granular samples, we focused on three measurements:

- the Angle of Repose (AOR). The AOR is the steepest angle of descent relative to the horizontal plane to which a material can pile before collapse (see 2.2.1);
- the compression strength. We measured the Young's Modulus (YM) for both confined and unconfined samples (see 2.2.2);
- the shear strength. We determined the shear yield stress of our samples when varying normal stresses were applied, and computed their Angle of Internal Friction (AIF) as well as bulk cohesion (see 2.2.3).

The YM, AIF, and bulk cohesion are properties that characterize the response of the soil to stress. Therefore, they have to be measured by applying stress to a sample. On the other hand, the AOR can be measured through observation and therefore, it can be directly detected on a planetary surface.

Unconfined measurements (AOR and unconfined compression) are applicable to material properties at the regolith surface layers, while confined measurements (confined compression and shear) are more applicable to the subsurface layers.

These experiments were performed on tabletop and at atmosphere. There was no control or measure of moisture content of the sample.

Table 1
Density and porosity values for our samples.

fine-fraction	Densities		Porosities	
	mm grains	cm grains	mm grains	cm grains
0	0.83 ±.11	0.71 ±.08	0.70 ±.04	.74 ±.05
25	0.85 ±.10	0.81 ±.10	0.69 ±.04	0.7 ±.03
50	0.89 ±.10	0.85 ±.10	0.68 ±.03	0.69 ±.03
75	0.92 ±.10	0.90 ±.10	0.66 ±.04	0.67 ±.03
100	0.92 ±.12	0.92 ±.12	.67 ±.05	.67 ±.05

2.1. Regolith simulants

2.1.1. Sample composition

To prepare our regolith samples, we aimed at reproducing the bulk mechanical properties of asteroid regolith. For this reason, we used simulant produced by the Exolith Lab mimicking the CI Orgueil meteoritic composition (Covey et al., 2016; Metzger et al., 2019).[1] This simulant has been used for other regolith studies and thoroughly characterized (Metzger et al., 2019; Brisset et al., 2022). Using specific metrics, such as grain and bulk densities, grain-size distribution, and volatile release, this simulant was shown to provide a good analog for carbonaceous-type asteroid surface regolith.

2.1.2. Grain-size distributions and sample preparation

For the purpose of our measurements, we prepared granular samples with grains in three size ranges: fines (fg, sieved to < 1 mm), millimeter (mm, sieved to sizes between 1 and 6 mm), and centimeter (cm, sieved to sizes between 6 and 20 mm). The fine grains were sieved directly out of the simulant batch, which comes as a powder.

Coarse grains were prepared by mixing this powder with water to obtain a mud-like mixture. From this mixture we formed cobbles (>10 cm), which were left to dry for 48 h before being placed into a dehydrator for an additional 24 h. The dried cobbles were then smashed into smaller grains using a hammer and sieved to the desired sizes.

In the present work, we focused on fine–coarse mixtures. For this, coarse grains (mm and cm) were mixed in with varying volumetric fine-fractions at 25%, 50%, and 75%. The mixing occurred by filling a mixing bowl with the varying volumes of fine and coarse grains. This simulant mixture was thoroughly stirred and poured into the sample container. Shaking of containers was limited to avoid grain sorting brought on by the Brazilian nut effect (Xie et al., 2012). Such a sample can be seen in Fig. 1.

As we are limited in our laboratory setting, we do not study large boulders. However, because of Eros (Robinson et al., 2002), Lutitia (Barucci et al., 2012), and Itokawa (Fujiwara et al., 2006), we infer the presence of fine–coarse mixtures on rubble-pile asteroids.

2.1.3. Sample density and porosity

We measured the mass and volume on 143 mixed samples. The computed sample densities and porosities are listed in Table 1, together with pure fine and pure coarse grain samples. These values are visualized in Fig. 2.

2.2. Measurements

For each measurement described below we took three data points. The standard deviation of these measurements was calculated and reported in the form of error bars on our data.

[1] https://exolithsimulants.com/collections/regolith-simulants/products/ci-carbonaceous-chondrite-simulant

Fig. 1. Example of a fine–coarse mixture of asteroid regolith simulant. This sample is composed of mm-sized grains mixed with a 25% fine-fraction. The picture was taken during an AOR measurement.

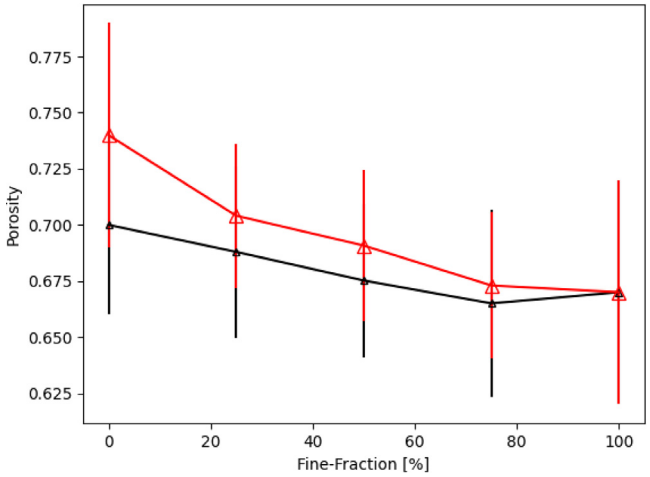

Fig. 2. Porosity plot for our samples. Data is shown for mm (black) and cm (red) grains in the coarse-fraction in relation to the fine-fraction.

2.2.1. Angle of repose

AOR measurements were completed using the fixed funnel method as described by Al-Hashemi and Al-Amoudi (2018). We poured 3.2 L of mixed material through a funnel and allowed it to naturally avalanche and create a pile. The sample was poured onto a raised metal cylinder to generate a well-defined pile. Pictures were taken at the base of the sample. This allowed for the measurement of the angle of the slope of the pile relative to the ground to be determined (Fig. 1).

2.2.2. Compression

We designed a compression setup with the ability to apply stress to both confined and unconfined samples for the purpose of determining their Young's Modulus (YM). The setup was operated by using an optical stage to lower a force gauge with a plate attachment in increments of .127 mm onto a sample in a container underneath. A measurement began when the force gauge experienced first contact and ended when the force gauge reached its limit at 200 N against the resistance from the sample.

The confined container was a cylinder of dimensions 50.8 mm inner diameter and 95.5 mm inner height. The plate attached to the force gauge was a similar diameter leaving only a small gap to allow it to move without friction during its descent.

The unconfined container was rectangular with inner dimensions 150 × 136 × 100 mm. With these dimensions, the container was about three times as large as the compression area, thus significantly reducing side wall effects during measurements. In both cases (confined and unconfined), compression measurements were performed using the same force gauge plate with a diameter of about 50.5 mm. Further details on these compression measurement setups are provided in Brisset et al. (2022).

As described in Brisset et al. (2022), the elastic response of our granular samples was not linear (Whitman, 1970). In our setup, we achieved compression stresses up to 30 kPa, which led to granular compression responses showing re-arrangement and hardening behavior (Omidvar et al., 2012). Our measurements were therefore best matched by an exponential fit of the type $\sigma = A\epsilon^B$ to our data, with σ being the stress in Pa applied and ϵ the sample strain (dimensionless). A and B are our measured constants, which we use to calculate the YM of our samples for a normal stress of 1 MPa: $E_{1\ \mathrm{MPa}} = A^{1/B}B(10^6)^{1-1/B}$ (Brisset et al., 2022). While this quantity is an arbitrary choice for a measurement of the samples' responses in compression, it allows for comparing the compressive strength of samples with various fine-fractions.

2.2.3. Shear strength

In order to measure shear strength, we placed the sample in a shear cell built as a container that was split at the middle height with both halves having a dimension of 89 × 89 × 57 mm. The bottom half could move along a frictionless rail using a linear actuator. The top half was held in place attached to a force gauge which measured the force experienced by the sample as it sheared. We applied an adjustable normal force to the top of the sample using weights. Each measurement started when the box halved and ended when shear yield was detected. Further details on this shear measurement setup can be found in Brisset et al. (2022).

In order to compute the AIF and bulk cohesion of the material, we performed shear measurements for six values of the applied normal stress. By determining the six shear yields associated with these normal stresses in the sample, we were able to generate a Mohr–Coulomb diagram (similar to the one shown in Brisset et al., 2022) . The Mohr–Coulomb formula is given as $\tau = \sigma\ \tan(\phi)$+c, where τ is the measured shear strength, ϕ is the applied normal stress, and c is the measured bulk cohesion of our sample. In this plot, the AIF, which is

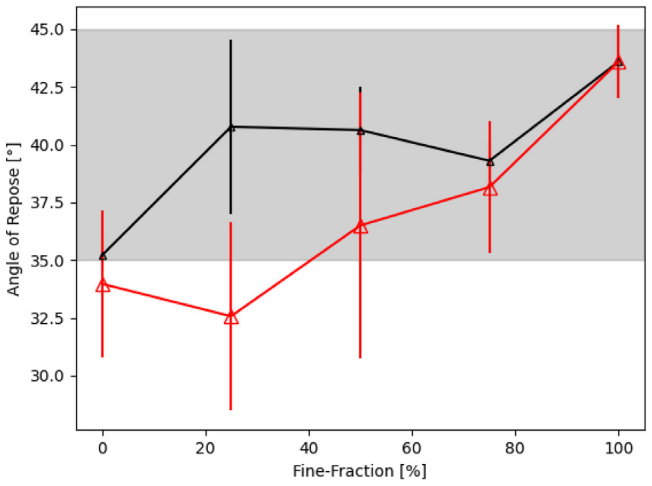

Fig. 3. AOR measurements for the same fine–coarse mixtures as in Figs. 5 and 6. Data is shown for mm (black) and cm (red) grains in the coarse-fraction in relation to the fine-fraction. The shaded region on the plot shows the values for Asteroid 2008 EV5, which also has a range of AOR values between 35° and 45° at mid-latitude (Scheeres, 2015).

Table 2
List of Angles of Repose described in Section 2.2.1 for all samples considered. Coefficient of friction (unitless) is determined from the tangent of the AOR (Al-Hashemi and Al-Amoudi, 2018).

fine-fraction	Angle of repose (°)		Coefficient of friction	
	mm grains	cm grains	mm grains	cm grains
0	35.20 ±.67	33.98 ±3.17	.71 ±.01	.67 ±.06
25	40.78 ±3.78	32.57 ±4.09	0.86 ±.07	0.64 ±.07
50	40.64 ±1.87	36.50 ±5.76	0.86 ±.03	0.74 ±.01
75	39.30 ±0.84	38.17 ±2.84	0.82 ±.01	0.79 ±.05
100	43.60 ±1.58	43.60 ±1.58	.95 ±.03	.95 ±.03

representative of a given failure-stress condition, is measured as the slope angle of the linear fit of shear yield versus normal stress. The bulk cohesion is the interaction force of a single material and is measured as the shear yield stress for zero normal stress (intersection of the linear fit with the Y-axis).

3. Results

3.1. Angle of repose

Fig. 1 shows an example of an AOR measurement. As expected from numerous other measurements on granular material (e.g. Al-Hashemi and Al-Amoudi, 2018), we see an overall increase in AOR with increasing fine-fractions in the samples. This is demonstrated in Fig. 3 with the corresponding values listed in Table 2. For mm-sized coarse grains, fine-fractions start dictating sample behavior as early as 25% fines. The stagnation seen for mm samples between 25% and 75% fine-fractions could be indicative of larger grains falling away during experimentation. Cm-sized grains see a gradual increase in AOR with increasing fine-fraction instead.

3.2. Compression

In Fig. 4, we show the evolution of the Young's Modulus (YM) with increasing fine-fraction. We find that the addition of an increasing fine-fraction leads to an increase in YM in mixed samples. However, the strongest samples are not the ones purely composed of fine grains. Mixtures of 25% coarse and 75% fines (a 75% fine-fraction) are the strongest samples in confined compression for both mm and cm samples (see Table 3). Confined samples are overall stronger than unconfined

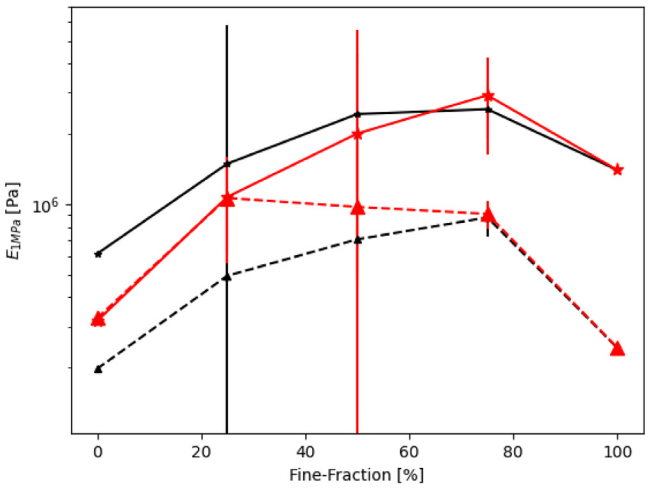

Fig. 4. Compression measurements for fine–coarse mixtures of asteroid regolith simulant. Young's Modulus for a normal stress of 1 MPa applied. Data is shown for mm (black) and cm (red) grains in the coarse-fraction as a function of the fine-fraction. The solid lines with star symbols are confined measurements and the dotted lines with triangle symbols are unconfined measurements.

Table 3
List of Young's Modulus as described in Section 2.2.2 for our asteroid simulant sample mixtures. The 0% and 100% fine-fraction values were determined in Brisset et al. (2022).

fine-fraction	E1MPA (Mpa)			
	Confined		Unconfined	
	mm grains	cm grains	mm grains	cm grains
0	.614 ±.011	.317 ±.012	.198 ±2.65e−4	.326 ±.008
25	1.49 ±4.32	1.07 ±.52	0.49 ±.01	1.06 ±.44
50	2.43 ±1.95	2.01 ±3.54	0.71 ±.02	0.97 ±.85
75	2.55 ±.65	2.92 ±1.30	0.88 ±.15	0.91 ±.12
100	1.4 ±.22	1.4 ±.22	.243 ±.011	.243 ±.011

Table 4
List of AIF and bulk cohesion values computed from our shear strength measurements (described in Section 2.2.3). The 0% and 100% fine-fraction values were determined in Brisset et al. (2022).

fine-fraction	Angle of internal friction (°)		Cohesion (Pa)	
	mm grains	cm grains	mm grains	cm grains
0	32.6 ±2.9	38.0 ±1.7	487 ±24	566 ±12
25	25.82 ±.90	41.50 ±9.00	473.81 ±5.64	423.44 ±65.48
50	24.66 ±5.76	29.14 ±10.67	483.10 ±32.46	401.37 ±42.41
75	22.75 ±1.41	24.93 ±2.94	412.22 ±11.18	302.05 ±21.26
100	24.2 ±1.1	24.2 ±1.1	384 ±8	384 ±8

ones, as seen in Brisset et al. (2022). This is expected due to the increased support the container side walls provide for force chains in the sample granular material.

3.3. Shear strength

In Fig. 5, we show the evolution of the Angle of Internal Friction (AIF) of samples with increasing fine-fraction. The shaded region in the figure is representative of AIF values needed to avoid rotational disruption. Though disruption limits can vary largely due to many factors, this shaded region is meant to serve as a guide for comparing our lab measurements to published AIF values. It should also highlight the potential of this material to aid a body in avoiding disruption as well as putting our measurements into context. For the cm samples, AIF values ranged from about 40° for the smallest fine-fractions to about 25° for the highest ones. For the mm samples, the AIF ranged from 33° to 25° with increasing fine-fraction. As the fine-fraction of a coarse sample is increased, the AIF decreases until it behaves like it is

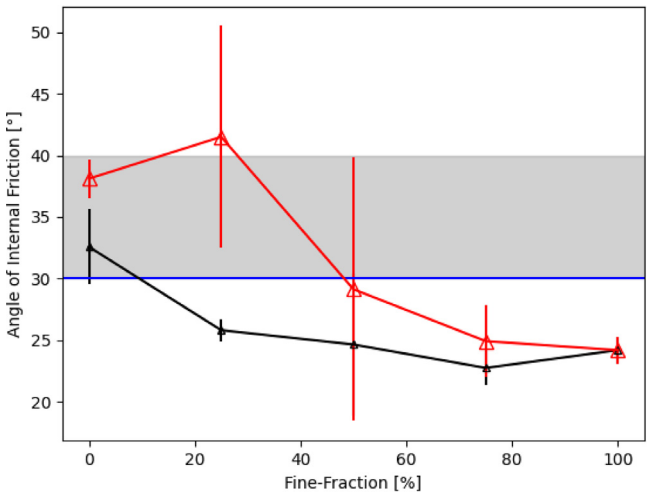

Fig. 5. Angle of Internal Friction (AIF) for our fine–coarse mixtures of asteroid regolith simulant. Data is shown for mm (black) and cm (red) grains in the coarse-fraction as a function of the fine-fraction. The shaded region is representative of the range of AIF values required to avoid rotational disruption as determined by Walsh (2018). The solid blue line is the minimum AIF value needed to avoid disruption (Holsapple, 2010).

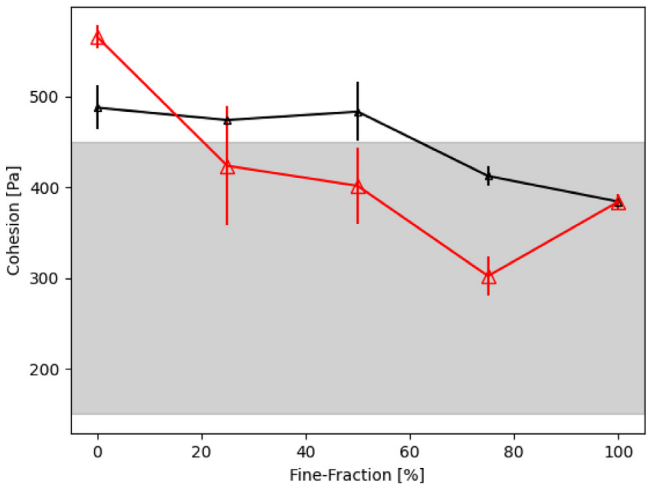

Fig. 6. Bulk cohesion for the same fine–coarse mixtures as in Fig. 5. Data is shown for mm (black) and cm (red) grains in the coarse-fraction as a function of the fine-fraction. The shaded region represents bulk cohesion values estimated for observed fast-rotator asteroids by Polishook et al. (2016).

entirely composed of fine grains (saturation). This happens for a 25% fine-fraction in mm samples while it requires a 75% fine-fraction for cm samples. It indicates that the fine grain fraction has more influence on the smaller mm-sized grains when mixed with fine grains when compared to the larger cm-sized grains. That is to say that mm samples began to behave more like pure fine samples at lower fine-fractions than cm samples did (see Table 4).

In Fig. 6, we show the evolution of the bulk cohesion with increasing fine-fraction. The shaded region represents strength measurements from Polishook et al. (2016), which studied fast rotators. It is meant to guide the eye for comparing our lab measurements to observed values from a space environment and to help put our measurements into context. Comparable to the AIF, bulk cohesion decreases with increasing fine-fraction for both mm and cm samples. In each of these sample types it ranged from about 500 Pa to 450 Pa and from about 600 Pa to 450 Pa, for mm samples and cm samples respectively. Opposite the AIF behavior, the cm samples seem to be more sensitive to the addition of a fine-fraction with their bulk cohesion decreasing notably for 25% fines compared to 75% fines required to see similar changes in the mm samples. The measurements reported here suggest that this material would support the avoidance of rotational disruption of an asteroid.

Both AIF and bulk cohesion measurements show that mixed fine–coarse samples become weaker in shear strength as the fine-fraction is increased. This is counter-intuitive as increasing fine-fractions are usually expected to strengthen granular samples (Sánchez and Scheeres, 2014).

From AIF and bulk cohesion measurements, we can deduce the samples' bulk tensile strengths. We find tensile strength values ranging from about 0.5 to approximately 1.1 kPa, supporting values used in simulations done by Zhang et al. (2018). Though these simulations treat tensile strength as a variable, our results indicate that the range of variables used in Zhang's simulations is relevant to fine–coarse regolith mixtures.

4. Discussion

Small body strength has been estimated several times using astronomical observations and numerical simulations. Polishook et al. (2016) focused on spin barriers of rubble-pile asteroids and deduced material strength based on their own observations of Asteroid (60716) 2000 GD65. Their findings indicate bulk cohesions around 150 to 450 Pa. These values are in good agreement with the range determined in our laboratory measurements (300 to 600 Pa). Additionally, we see overlap between our laboratory measurements and simulation work regarding angle of internal friction (AIF) (see Walsh, 2018), as well as angle of repose (AOR) measurements from the surface of an asteroid (see Scheeres, 2015). The good agreement of our work with these observations and simulations indicates that our table-top measurements are relevant to the understanding of regolith behavior on and inside small asteroids despite the differences between the natural bodies and laboratory environments discussed throughout Section 2.

4.1. Surface strength of rubble piles

According to Harris et al. (2009), the asteroid 1999 KW4 has what is described as a "constant" surface slope (equivalent to the AOR of surface material) of approximately 35° in mid-latitude regions. Scheeres (2015) reports the same mid-latitude region as a "constant" slope of approximately 40°. Scheeres (2015) also reports an AOR range (35°–45°) for a comparable region of a similar asteroid, Asteroid 2008 EV5.

Scheeres et al. (2019) report a similar range of slopes for the boulder populated regions of Near Earth Asteroid 101955 Bennu (Bennu). These regions show angles as high as 46°. This wide range of surface slopes is quite similar to those reported in Section 3 (Fig. 3). Higher angle measurements are seen mostly toward the poles of Bennu indicating a potential for increased fines toward the poles. Surface slopes toward the equator are on the lower end of the reported range except on crater rims. Impacts that cause craters often cause an excavation of materials from beneath the surface (Melosh, 2011). Though the surface is coarse and seemingly depleted of fine grains in certain areas, our AOR measurements suggest the presence of fine grain materials just beneath the surface in the shallow interior. This is supported by the findings reported by Lauretta et al. (2022). Additionally, the increased AOR along the rim of craters along the equator could be a result of fine-course mixing resulting from the impact. While reduced gravity is influential and is not considered in this study, many factors can influence the AOR (Al-Hashemi and Al-Amoudi, 2018; Scheeres, 2015). Though surface slopes are known to increase in lower gravity environments (Kleinhans et al., 2011), we do not see this trend on Bennu with certain areas containing averages below 20° (Scheeres et al., 2019). This is likely a result of the active surface processes such as seismic shaking and mass movement described in Jawin et al. (2022).

Comparatively, we are overlapping a bit by chance with the AOR values reported by Scheeres et al. (2019). However, if you look at the comparable values we can draw some conclusions about the data. For our samples with larger coarse grains (cm samples), larger fractions of fine grains (fine-fraction > 50%) yielded notably steeper AOR values. This could be an indicator that for areas experiencing more activity and maintaining higher relative slopes, such as crater rims, there is an increased presence of fine grains.

4.2. Internal structure of rubble piles

The Drucker–Prager failure criterion defines a constant, s, as follows:

$$s = \frac{2sin\phi}{\sqrt{3}(3 - sin\phi)}$$

that can be related to the AIF (ϕ) for material in a small body. As the AIF increases, so does the constant, s. Here, a failure criterion is a measure of the stress required to cause a failure, so a higher AIF leads to resistance of the sample to fail. Holsapple (2010) uses this to link the AIF to the failure behavior of an asteroid. Following this, Walsh (2018) finds that, to be consistent with the observed population of small asteroids, the AIF of rubble-pile asteroids to avoid failure ranges from 30° to 40°. The best matching results were toward the upper end of that range with values around 40°. In the similar AIF values we find in our laboratory study, the larger values are achieved in cm samples with low fine-fractions. This argues for the interiors of rubble-pile asteroids possibly containing low fine-fractions (≤25%). Interestingly, we see that this behavior differs from that of the AOR.

Numerical simulations and observations (i.e. Holsapple, 2010; Rozitis et al., 2014; Sánchez and Scheeres, 2014) have demonstrated the need for small fast-rotating rubble piles to have a cohesive strength in addition to shear strength to avoid failure. Sánchez and Scheeres (2014) describe increasing fine-fraction as one method of increasing cohesion of the material. Our findings do not support this hypothesis as we have found that, in confined environments, bulk cohesion weakens with increasing fine-fraction. The bulk cohesion measurements reported here suggest that this material would support the avoidance of rotational disruption of fast rotators, but that larger grains might be more prominent in the interior to do so. We speculate here that one possible reason for this difference is the erosion fine grains undergo during the shearing process from grinding in the presence of coarse grains. This erosion circularizes grains and allows them to serve as a lubricant for the larger grains in the sample rather than cement them in place. Numerical work, so far, is not taking into consideration how the mechanical interaction between large and small grains might modify them. Holsapple (2010) determined in his simulations that most rubble-pile body shapes are possible and can avoid failure with an AIF of 30°.

4.3. Bulk cohesion

Hirabayashi et al. (2015) report minimum cohesion measurements of 75–85 Pa to avoid failure in the asteroid 1950 AD. Additionally, Hirabayashi et al. (2014) report possible cohesive strength values for Main Belt Comet P/2013 R3 to be 40–210 Pa based on its breakup event which was believed to have occurred between February 2013 and September 2013 (Jewitt et al., 2014). It was observed by the Hubble Space telescope from October 2013 to February 2014 (Jewitt et al., 2017). In our laboratory measurements, we find cohesion values larger than minimum values required to prevent rotational break-up reported in the literature indicating that our experiments are closely aligned with observations.

4.4. Compression behavior

Our measurements also produced Young's Modulus (YM) values for fine–coarse regolith mixtures. As expected (from Brisset et al., 2022; Zhang et al., 2022), we found that in confined environments the YM was stronger than in unconfined environments. Intuitively, pure fine grain samples would be expected to yield the strongest YM values. There is a correlation between the compression strength of a sample and that sample's porosity prior to compaction. Samples with higher porosities are more likely to experience failures (Wikberg and Alderborn, 1991). Interestingly, we found that the highest YM values are measured in fine–coarse mixtures rather than pure fine grain samples. We speculate this is because the larger grain samples are stiffened by the presence of fine grains due to the reduction of space between the grains (thereby reducing porosity in the sample) preventing coarse grains from moving into void spaces. This phenomenon occurs until the sample is saturated with fine grains and begins behaving like a pure fine grain sample.

5. Summary and conclusion

In this paper, we present laboratory measurements of bulk mechanical properties of fine–coarse mixtures. These samples were prepared using a varying fine grain percentage by volume of the sample and the grains were a high fidelity asteroid soil simulant. The measurements included angle of repose (AOR), Young's Modulus (YM), angle of internal friction (AIF), cohesion, and tensile strength. All measurements show a clear dependency on the fine grain percentage. In AOR, the coarse samples are strengthened by the addition of fine grains all the way to the pure fine sample. YM (both confined and unconfined) increases with increasing fine-fraction, but only to a point. In all compression cases the strongest sample was a fine–coarse mixture. Both AIF and bulk cohesion decreased with increasing fine-fraction likely due to the decrease in interlocking of irregular shaped grains brought on by the increasing presence of fines (Brisset et al., 2022).

We observe that coarse grains are strengthened in compression strength with the presence of fine grains but are weakened in shear strength. The fine grains reduce the void space available to the coarse grains causing a fortification of the coarse grains when introduced to compressive stresses. However, the presence of fine grains reduces granular interlocking between coarse grains in cases of shear stress. We conclude that the presence of fine grains help a rubble-pile asteroid to avoid disruption from impacts, but increases the chance of spin deformation and rotational disruption in varying circumstances.

CRediT authorship contribution statement

Christopher Cox: Conceptualization, Data curation, Formal analysis, Investigation, Methodology, Project administration, Software, Supervision, Validation, Visualization, Writing – original draft, Writing – review & editing. **Julie Brisset:** Formal analysis, Funding acquisition, Methodology, Project administration, Resources, Supervision, Writing – original draft, Writing – review & editing. **Aracelis Partida:** Data curation, Investigation. **Alexander Madison:** Formal analysis, Investigation. **Olivia Bitcon:** Investigation.

Declaration of competing interest

The authors declare that they have no known competing financial interests or personal relationships that could have appeared to influence the work reported in this paper.

Data availability

Data will be made available on request.

Acknowledgments

This work was funded by the National Science Foundation, award # 1830609.

References

Al-Hashemi, H.M.B., Al-Amoudi, O.S.B., 2018. A review on the angle of repose of granular materials. Powder Technol. 330, 397–417.

Barucci, M., Belskaya, I., Fornasier, S., Fulchignoni, M., Clark, B., Coradini, A., Capaccioni, F., Dotto, E., Birlan, M., Leyrat, C., et al., 2012. Overview of Lutetia's surface composition. Planet. Space Sci. 66 (1), 23–30.

Brisset, J., Sánchez, P., Cox, C., Corraliza, D., Hatchitt, J., Madison, A., Miletich, T., 2022. Asteroid regolith strength: Role of grain size and surface properties. Planet. Space Sci. 220, 105533.

Busch, M.W., Ostro, S.J., Benner, L.A., Brozovic, M., Giorgini, J.D., Jao, J.S., Scheeres, D.J., Magri, C., Nolan, M.C., Howell, E.S., et al., 2011. Radar observations and the shape of near-Earth asteroid 2008 EV5. Icarus 212 (2), 649–660.

Covey, S., Lewis, J., Metzger, P., Britt, D., Wiggins, S., 2016. Simulating the surface morphology of a carbonaceous chondrite asteroid. In: Earth & Space Conference. pp. 11–15.

Fujiwara, A., Kawaguchi, J., Yeomans, D., Abe, M., Mukai, T., Okada, T., Saito, J., Yano, H., Yoshikawa, M., Scheeres, D., et al., 2006. The rubble-pile asteroid Itokawa as observed by Hayabusa. Science 312 (5778), 1330–1334.

Harris, A.W., Fahnestock, E.G., Pravec, P., 2009. On the shapes and spins of "rubble pile" asteroids. Icarus 199 (2), 310–318.

Hirabayashi, M., Sánchez, D.P., Scheeres, D.J., 2015. Internal structure of asteroids having surface shedding due to rotational instability. Astrophys. J. 808 (1), 63.

Hirabayashi, M., Scheeres, D.J., Sánchez, D.P., Gabriel, T., 2014. Constraints on the physical properties of main belt comet P/2013 R3 from its breakup event. Astrophys. J. Lett. 789 (1), L12.

Holsapple, K.A., 2007. Spin limits of solar system bodies: From the small fast-rotators to 2003 EL61. Icarus 187 (2), 500–509.

Holsapple, K.A., 2010. On YORP-induced spin deformations of asteroids. Icarus 205 (2), 430–442.

Jawin, E., McCoy, T., Walsh, K., Connolly, Jr., H., Ballouz, R.L., Ryan, A., Kaplan, H., Pajola, M., Hamilton, V., Barnouin, O., et al., 2022. Global geologic map of asteroid (101955) Bennu indicates heterogeneous resurfacing in the past 500,000 years. Icarus 381, 114992.

Jewitt, D., Agarwal, J., Li, J., Weaver, H., Mutchler, M., Larson, S., 2014. Disintegrating asteroid P/2013 R3. Astrophys. J. Lett. 784 (1), L8.

Jewitt, D., Agarwal, J., Li, J., Weaver, H., Mutchler, M., Larson, S., 2017. Anatomy of an asteroid breakup: the case of P/2013 R3. Astron. J. 153 (5), 223.

Kleinhans, M., Markies, H., De Vet, S., In't Veld, A., Postema, F., 2011. Static and dynamic angles of repose in loose granular materials under reduced gravity. J. Geophys. Res.: Planets 116 (E11).

Lauretta, D., Adam, C., Allen, A., Ballouz, R.L., Barnouin, O., Becker, K., Becker, T., Bennett, C., Bierhaus, E., Bos, B., et al., 2022. Spacecraft sample collection and subsurface excavation of asteroid (101955) Bennu. Science 377 (6603), 285–291.

Lauretta, D., DellaGiustina, D., Bennett, C., Golish, D., Becker, K., Balram-Knutson, S., Barnouin, O., Becker, T., Bottke, W., Boynton, W., et al., 2019. The unexpected surface of asteroid (101955) Bennu. Nature 568 (7750), 55–60.

Melosh, H.J., 2011. Planetary Surface Processes. In: Cambridge Planetary Science, Cambridge University Press, http://dx.doi.org/10.1017/CBO9780511977848.

Metzger, P.T., Britt, D.T., Covey, S., Schultz, C., Cannon, K.M., Grossman, K.D., Mantovani, J.G., Mueller, R.P., 2019. Measuring the fidelity of asteroid regolith and cobble simulants. Icarus 321, 632–646.

Michikami, T., Honda, C., Miyamoto, H., Hirabayashi, M., Hagermann, A., Irie, T., Nomura, K., Ernst, C.M., Kawamura, M., Sugimoto, K., et al., 2019. Boulder size and shape distributions on asteroid Ryugu. Icarus 331, 179–191.

Omidvar, M., Iskander, M., Bless, S., 2012. Stress-strain behavior of sand at high strain rates. Int. J. Impact Eng. 49, 192–213.

Perry, M., Barnouin, O., Daly, R., Bierhaus, E., Ballouz, R.L., Walsh, K., Daly, M., DellaGiustina, D., Nolan, M., Emery, J., et al., 2022. Low surface strength of the asteroid Bennu inferred from impact ejecta deposit. Nat. Geosci. 15 (6), 447–452.

Polishook, D., Moskovitz, N., Binzel, R.P., Burt, B., DeMeo, F.E., Hinkle, M.L., Lockhart, M., Mommert, M., Person, M., Thirouin, A., et al., 2016. A 2 km-size asteroid challenging the rubble-pile spin barrier–A case for cohesion. Icarus 267, 243–254.

Robinson, M., Thomas, P., Veverka, J., Murchie, S., Wilcox, B., 2002. The geology of 433 eros. Meteorit. Planet. Sci. 37 (12), 1651–1684.

Rozitis, B., MacLennan, E., Emery, J.P., 2014. Cohesive forces prevent the rotational breakup of rubble-pile asteroid (29075) 1950 DA. Nature 512 (7513), 174–176.

Sánchez, P., Scheeres, D.J., 2014. The strength of regolith and rubble pile asteroids. Meteorit. Planet. Sci. 49 (5), 788–811.

Scheeres, D.J., 2015. Landslides and mass shedding on spinning spheroidal asteroids. Icarus 247, 1–17.

Scheeres, D.J., Hartzell, C.M., Sánchez, P., Swift, M., 2010. Scaling forces to asteroid surfaces: The role of cohesion. Icarus 210 (2), 968–984.

Scheeres, D., McMahon, J., French, A., Brack, D., Chesley, S., Farnocchia, D., Takahashi, Y., Leonard, J., Geeraert, J., Page, B., et al., 2019. The dynamic geophysical environment of (101955) Bennu based on OSIRIS-REx measurements. Nat. Astron. 3 (4), 352–361.

Scheeres, D.J., Sánchez, P., 2018. Implications of cohesive strength in asteroid interiors and surfaces and its measurement. Prog. Earth Planetary Sci. 5 (1), 1–10.

Walsh, K.J., 2018. Rubble pile asteroids. Annu. Rev. Astron. Astrophys. 56, 593–624.

Watanabe, S., Hirabayashi, M., Hirata, N., Hirata, N., Noguchi, R., Shimaki, Y., Ikeda, H., Tatsumi, E., Yoshikawa, M., Kikuchi, S., et al., 2019. Hayabusa2 arrives at the carbonaceous asteroid 162173 Ryugu—A spinning top–shaped rubble pile. Science 364 (6437), 268–272.

Whitman, R.V., 1970. The response of soils to dynamic loadings; report 26, final report. Technical Report, MASSACHUSETTS INST OF TECH CAMBRIDGE DEPT OF CIVIL ENGINEERING.

Wikberg, M., Alderborn, G., 1991. Compression characteristics of granulated materials. IV. The effect of granule porosity on the fragmentation propensity and the compatibility of some granulations. Int. J. Pharmaceut. 69 (3), 239–253.

Xie, Z.A., Wu, P., Zhang, S.P., Chen, S., Jia, C., Liu, C.P., Wang, L., 2012. Separation patterns between Brazilian nut and reversed Brazilian nut of a binary granular system. Phys. Rev. E 85 (6), 061302.

Zhang, Y., Michel, P., Barnouin, O.S., Roberts, J.H., Daly, M.G., Ballouz, R.L., Walsh, K.J., Richardson, D.C., Hartzell, C.M., Lauretta, D.S., 2022. Inferring interiors and structural history of top-shaped asteroids from external properties of asteroid (101955) Bennu. Nature Commun. 13 (1), 1–12.

Zhang, Y., Richardson, D.C., Barnouin, O.S., Michel, P., Schwartz, S.R., Ballouz, R.L., 2018. Rotational failure of rubble-pile bodies: influences of shear and cohesive strengths. Astrophys. J. 857 (1), 15.